Nonlinear Noise-Induced Transitions in Active Rotator Model

Seunghwan Kim, Seon Hee Park, and Chang Su Ryu

CONTENTS

ABSTRACT

We investigate noise-induced transitions in active rotator model with a fluctuating threshold in the presence of an additive noise. The fluctuation of the threshold depends on the additive noise in a nonlinear fashion. In the white-noise limit of the fluctuation, the Fokker-Planck equation of the system reduces to that of the system with correlated linear fluctuation implying that the nonlinearity may be transformed into the correlation of linear noises. We also investigate the system with a nonlinear colored noise which depends on the additive noise as its square. The system shows a single peak, two peaks, and three peaks in its steady state probability distribution according to the noise intensities and the correlation time whose change leads to peak-creating, peak-splitting, and peak-merging transitions.

I. INTRODUCTION

In sensory processing the linking of sensory inputs across multiple receptive fields is a fundamental task to identify distinct objects, segment them from each other, and separate them from background. This linkage is difficult to approach within the framework of most current artificial neural network models because they use only the levels of activity in individual neurons to encode information. To overcome this difficulty the model based on the dynamics of biological neurons has been suggested in which global properties of stimuli are identified through correlations in the temporal firing patterns of different neurons [1]. Recent experiments provided support to this concept showing that neurons in the primary visual cortex of the cat can exhibit oscillatory responses [2], [3]. The existence of temporal synchronization over relatively large distances in the cortex suggests that the processing of information is a cooperative process of neurons with different receptive fields.

Oscillations of neuronal activity in the visual cortex and their potential role in computation have been the topic of much recent investigation. A phase oscillator model which consists of neurons with oscillatory outputs was suggested to understand the temporal and spatial coherence of the oscillations [4]. The phase oscillators have been studied extensively as a model system to understand dynamics of various systems such as Josephson-junctions [5], chemical reactions [6], and charge-density waves [7], [8]. Active rotators have been studied as a phase model of either limit-cycle oscillators or excitable elements [9]. The active rotator model has been derived to study phase fluctuations of a self-sustained Van der Paul oscillator [10] which is a reduced model of the Hodgkin-Huxley model, a well-known physiological neuron model. The active rotator shows a peculiar dynamics that it is in a fixed point for driving force less than threshold and in a moving state for driving force larger than threshold. Recently the complex oscillating neural network model was suggested as a model for flexible pattern recognition [11], [12]. The model is based on the self-organization of a spatio-temporal pattern in an oscillating network. The flexibility of pattern recognition is caused from the flexibility of connections by entrainment and from the stability of dynamic patterns for deformation. The model showed the possibility of flexible pattern recognition by the oscillating neural network.

The question on the role of noise in a dynamical system has been raised continuously. Transitions induced by a multiplicative noise in low-dimensional dynamical systems are by now a familiar phenomenon [13], but the multiplicative noise in spatially distributed and/or high-dimensional systems remains the focus of current research [14], [15]. While the noise-induced nonequilibrium phase transitions in the spa-

tially distributed systems are characterized by the symmetry-breaking transition, the noise-induced transitions in the low-dimensional dynamical systems are characterized by the qualitative change of the shape of the system's probability distribution. The active rotators with an additive noise show the transition from moving (excited) state to stationary (inhibited) state at a critical noise intensity. Noise-induced transitions in the model with fluctuating threshold were investigated showing interesting nonequilibrium phenomena [16]-[22]. In [16] and [17], the authors considered the linear fluctuations of the threshold uncorrelated or correlated to the additive noise. The nonlinear fluctuations of the threshold are more realistic and general for the excitable systems such as neurons. Thus, the study of the nonlinear fluctuation effect of the threshold on the active rotator model is required.

In this paper we investigate noise-induced transitions in the active rotator model with a fluctuating threshold in the presence of an additive noise. The noise-induced transitions are characterized by the change of number of peaks in the system's probability distribution. We consider the fluctuation of the threshold which depends on the additive noise in a nonlinear fashion. In the white-noise limit of the fluctuation we obtain the effective Fokker-Planck equation of the system which has the same form with that of the system with correlated linear fluctuations. This implies that the nonlinearity may be transformed into the correlation of the linear noises. We also investigate the system with a nonlinear colored noise which depends on the additive noise as its square. The colored noise is given by the Ornstein-Uhlenbeck process with a finite correlation time. In this case the system shows a single peak, two peaks, and three peaks in its steady state probability distribution according to the noise intensities and the correlation time. The change of the noise intensities and the correlation time leads to peak-creating, peak-splitting, and peak-merging transitions. We present phase portraits for various parameter values.

In the following section we describe the model under study in this paper. Section III is devoted to present the effective Fokker-Planck equation for the nonlinear fluctuations in the white-noise limit. In Sec. IV we present phase portraits obtained by the numerical simulations for the system with the nonlinear colored noise. Implication of the nonequilibrium phenomena of the system is discussed with summarized results in Sec. V.

II. MODEL

Active rotator model under study is expressed by the equation of motion [9]

$$\frac{d\phi}{dt} = \omega - b\sin\phi,$$

where ϕ is the phase of the rotator, ω is the intrinsic frequency indicating the driv-

ing force, and b represents the threshold of the system. In the steady state ϕ dwells on two phases. When $|b/\omega| > 1$, the rotator is at the stable fixed point, $\phi = \phi_0 \equiv \sin^{-1}(\omega/b)$. When $|b/\omega| < 1$, the system is on the moving phase with frequency $\sqrt{\omega^2 - b^2}$. The threshold b characterizes the system whether it is on the stationary state or on the moving state.

If the system is coupled to a fluctuating environment, the threshold then may be assumed to be a stochastic quantity, which implies

$$b \to b + \Delta,$$

where Δ is a fluctuation of the threshold with mean zero. In this paper we consider the fluctuation which depends on an additive noise in a nonlinear fashion. Then, the equation of motion of the system is given by

$$\frac{d\phi}{dt} = \omega - \{b + \Delta[\zeta(t)]\}\sin\phi + \sigma_A \zeta(t), \qquad (1)$$

where $\zeta(t)$ is a Gaussian noise characterized by mean zero and unit variance and $\Delta[\zeta(t)]$ is a nonlinear function of $\zeta(t)$. In (1) σ_A measures the intensity of the additive noise. The additive noise $\zeta(t)$ may come from thermal fluctuation. The thermal fluctuation is an intrinsic noise which always exists at finite temperature. It is realistic to assume that the threshold also fluctuates due to the thermal fluctuation leading to the dependence of $\Delta[\zeta]$ on $\zeta(t)$.

To study colored-noise effect on the system we take the additive noise as the Ornstein-Uhlenbeck process given by the stochastic differential equation

$$\frac{d\zeta}{dt} = -\zeta + \xi(t) \qquad (2)$$

with a white noise process $\xi(t)$ characterized by

$$\langle \xi(t) \rangle = 0,$$
$$\langle \xi(t)\xi(t') \rangle = \delta(t - t').$$

According to [13] and [23], to speed up the system we rescale time t and the fluctuation

$$\eta(\phi,\ \zeta(t)) \equiv -\Delta[\zeta(t)]\sin\phi + \sigma_A \zeta(t) \qquad (3)$$

as

$$\eta_\epsilon(\phi,\ \zeta_\epsilon(t)) = \frac{1}{\epsilon}\eta\left(\phi,\ \zeta\left(\frac{t}{\epsilon^2}\right)\right),$$
$$\zeta_\epsilon(t) = \zeta\left(\frac{t}{\epsilon^2}\right) \qquad (4)$$

with correlation time $\tau \equiv \epsilon^2$. With the transformation (4), we obtain the following stochastic differential equations

$$\frac{d\phi}{dt} = \omega - b\sin\phi - \frac{\Delta[\zeta_\epsilon(t)]\sin\phi - \sigma_A\zeta_\epsilon(t)}{\epsilon},$$
$$\frac{d\zeta_\epsilon}{dt} = -\frac{\zeta_\epsilon}{\epsilon^2} + \frac{\xi(t)}{\epsilon}. \qquad (5)$$

In the limit of $\epsilon \to 0$, (5) gives the white-noise limit of (1) defined as the wide-band limit of fluctuation $\eta(\phi,\ \zeta)$ [24]. The power spectral density $S(\phi,\ \Omega)$ of $\eta(\phi,\ \zeta)$ is defined by

$$S(\phi,\ \Omega) = \int_{-\infty}^{\infty} \exp[i\Omega_s] R(\phi,\ s) ds$$

with

$$R(\phi,\ s) = \langle \eta(\phi,\ \zeta(t))\eta(\phi,\ \zeta(t+s))\rangle.$$

By the transformation (4) $R(\phi,\ s)$ transforms into

$$R_\epsilon(\phi,\ s) = \frac{1}{\epsilon^2} R\left(\phi,\ \frac{s}{\epsilon^2}\right).$$

In the limit of $\epsilon \to 0$, $R_\epsilon(\phi, s)$ reduces to

$$\int_{-\infty}^{\infty} R(\phi,\ t)dt\delta(s)$$

leading to the uniform $S(\phi,\ \Omega)$ and thus wide-band limit of $\eta(\phi,\ \zeta)$.

The macroscopic behavior of the system corresponding to the stochastic differential equation (5) can be described by the probability distribution $P_\epsilon(\phi,\ \zeta_\epsilon,\ t)$ of ϕ and ζ_ϵ at time t, whose evolution is governed by the Fokker-Planck equation [25]

$$\frac{\partial P_\epsilon(\phi,\ \zeta_\epsilon,\ t)}{\partial t} = \left(\frac{1}{\epsilon^2}F_1 + \frac{1}{\epsilon}F_2 + F_3\right) \times P_\epsilon(\phi,\ \zeta_\epsilon,\ t) \tag{6}$$

with differential operators

$$F_1 \equiv \frac{\partial}{\partial \zeta_\epsilon}\zeta_\epsilon + \frac{1}{2}\frac{\partial^2}{\partial \zeta_\epsilon^2},$$
$$F_2 \equiv -\frac{\partial}{\partial \phi}\eta(\phi,\ \zeta_\epsilon),$$
$$F_3 \equiv -\frac{\partial}{\partial \phi}(\omega - b\sin\phi).$$

In the following sections, we investigate probability distribution

$$P_\epsilon(\phi) \equiv \int_{-\infty}^{\infty} P_\epsilon(\phi,\ \zeta_\epsilon,\ t)d\zeta_\epsilon$$

of ϕ at the steady state given in the limit of $t \to \infty$.

III. WHITE-NOISE LIMIT

To obtain the effective Fokker-Planck equation in the white-noise limit, we expand $P_\epsilon(\phi,\ \zeta_\epsilon,\ t)$ as a series of ϵ:

$$P_\epsilon(\phi,\ \zeta_\epsilon,\ t) = P_{\zeta_\epsilon}(\zeta_\epsilon)[P(\phi,\ t) + \epsilon r_1(\phi,\ \zeta_\epsilon,\ t) + \epsilon^2 r_2(\phi,\ \zeta_\epsilon,\ t) + \cdots],$$

where $P(\phi,\ t)$ represents the probability distribution in the white-noise limit, i.e., in the limit of $\epsilon \to 0$. Then up to zeroth-order of ϵ, (6) gives the following equations:

$$F_1 P_{\zeta_\epsilon}(\zeta_\epsilon) = 0, \tag{7}$$
$$F_1 P_{\zeta_\epsilon}(\zeta_\epsilon) r_1(\phi,\zeta_\epsilon,t) = -P_{\zeta_\epsilon}(\zeta_\epsilon) F_2 P(\phi,t), \tag{8}$$
$$F_1 P_{\zeta_\epsilon}(\zeta_\epsilon) r_2(\phi,\zeta_\epsilon,t) = P_{\zeta_\epsilon}(\zeta_\epsilon)\left[\frac{\partial P(\phi,t)}{\partial t} - F_2 r_1(\phi,\zeta_\epsilon,t) - F_3 P(\phi,t)\right]. \tag{9}$$

Equation (7) has the solution $P_{\zeta_\epsilon}(\zeta_\epsilon) = \frac{1}{\sqrt{\pi}} \exp\left[-\zeta_\epsilon^2\right]$ which gives the probability distribution for the Ornstein-Uhlenbeck process (2) in the steady state.

The solution of (8), $r_1(\phi,\ \zeta_\epsilon,\ t)$ consists of a homogeneous solution $H(\phi,\ t)$ and a particular solution $G(\phi,\ \zeta_\epsilon,\ t)$ leading to

$$r_1(\phi,\ \zeta_\epsilon,\ t) = H(\phi,\ t) + G(\phi,\ \zeta_\epsilon,\ t).$$

After the transformation of $F_1 P_{\zeta_\epsilon}(\zeta_\epsilon)$ as

$$F_1 P_{\zeta_\epsilon}(\zeta_\epsilon) = \frac{1}{2}\frac{\partial}{\partial \zeta_\epsilon} P_{\zeta_\epsilon}(\zeta_\epsilon)\frac{\partial}{\partial \zeta_\epsilon}$$

we obtain the particular solution $G(\phi,\ \zeta_\epsilon,\ t)$ by double integrations as

$$G(\phi,\ \zeta_\epsilon,\ t) = -2\int_0^{\zeta_\epsilon} d\zeta_\epsilon' \exp\left[\zeta_\epsilon'^2\right] \times \int_{\zeta_\epsilon'}^{\infty} d\zeta_\epsilon'' \exp\left[-\zeta_\epsilon''^2\right] \frac{\partial}{\partial \phi}[\eta(\phi,\ \zeta_\epsilon)P(\phi,\ t)].$$

Here, we take the appropriate reference points of the integrations to avoid divergence.

After the integration over ζ_ϵ, (9) reduces to

$$\frac{\partial P(\phi,\ t)}{\partial t} = -\frac{\partial}{\partial \phi}\Bigg[\int_{-\infty}^{\infty} d\zeta_\epsilon P_{\zeta_\epsilon}(\zeta_\epsilon)\eta(\phi,\ \zeta_\epsilon) \times\{H(\phi,\ t)+G(\phi,\ \zeta_\epsilon,\ t)\} +(\omega - b\sin\phi)P(\phi,\ t)\Bigg]. \quad (10)$$

Since the fluctuation $\eta(\phi,\ \zeta_\epsilon)$ given by (3) has zero mean,

$$\int_{-\infty}^{\infty} d\zeta_\epsilon P_{\zeta_\epsilon}(\zeta_\epsilon)\eta(\phi,\ \zeta_\epsilon) = 0.$$

Thus, the first term of right-hand side of (10) divided into two terms as

$$-\frac{2}{\sqrt{\pi}}\frac{\partial}{\partial\phi}\int_{-\infty}^{\infty} d\zeta_\epsilon \exp\left[-\zeta_\epsilon^2\right]\left[\frac{\partial\eta(\phi,\ \zeta_\epsilon)}{\partial\phi} -\frac{\partial}{\partial\phi}\eta(\phi,\ \zeta_\epsilon)\right]\int_0^{\zeta_\epsilon} d\zeta_\epsilon' \exp\left[\zeta_\epsilon^2\right] \times\int_{\zeta_\epsilon'}^{\infty} d\zeta_\epsilon'' \exp\left[-\zeta_\epsilon''^2\right]\eta(\phi,\ \zeta_\epsilon''),$$

leading to the following effective Fokker-Planck equation

$$\frac{\partial P(\phi,\ t)}{\partial t} = -\frac{\partial}{\partial\phi}[\{\omega - b\sin\phi + f(\phi)\}P(\phi,\ t)] +\frac{1}{2}\frac{\partial^2}{\partial\phi^2}[g(\phi)P(\phi,\ t)] \quad (11)$$

with

$$f(\phi) = \frac{1}{2}\Delta_1\cos\phi\sin\phi - \frac{1}{2}\sigma_A\Delta_2\cos\phi,$$
$$g(\phi) = \Delta_1\sin^2\phi - 2\sigma_A\Delta_2\sin\phi + \sigma_A^2, \quad (12)$$

where

$$\Delta_1 = \frac{4}{\sqrt{\pi}}\int_{-\infty}^{\infty} d\zeta \exp\left[-\zeta^2\right]\Delta[\zeta]\int_0^{\zeta} d\zeta' \exp[\zeta'^2] \times\int_{\zeta'}^{\infty} d\zeta'' \exp\left[-\zeta''^2\right]\Delta[\zeta''],$$

$$\Delta_2 = \frac{2}{\sqrt{\pi}}\int_{-\infty}^{\infty} d\zeta \exp\left[-\zeta^2\right]\zeta\Delta[\zeta].$$

In (11) $f(\phi)$ is the noise-induced drift force and $g(\phi)$ is the diffusion coefficient. In the case of linear fluctuating threshold with $\Delta[\zeta] = \sigma_M\zeta$, i.e., $\eta(\phi,\ \zeta) = -(\sigma_M\sin\phi - \sigma_A)\zeta$, $\Delta_1 = \sigma_M^2$ and $\Delta_2 = \sigma_M$ leading to the well-known Fokker-Planck equation for the linear noise with

$$f(\phi) = \frac{1}{2}\sigma_M\cos\phi(\sigma_M\sin\phi - \sigma_A),$$
$$g(\phi) = (\sigma_M\sin\phi - \sigma_A)^2.$$

The effective Fokker-Planck equation (11) has the same form as that for the system with correlated linear fluctuating threshold to the additive noise. If $\Delta[\zeta(t)]$ is replaced by a term proportional to a Gaussian white noise $\xi(t)$ with mean zero and unit variance and correlated to $\zeta(t)$ by

$$\langle\xi(t)\zeta(t')\rangle = R\delta(t-t'),$$

the equation of motion (1) is written by

$$\frac{d\phi}{dt} = \omega - [b + \sigma_M\xi(t)]\sin\phi + \sigma_A\zeta(t), \quad (13)$$

where σ_M measures the intensity of the multiplicative noise. Since sum of two Gaussian white noises is also a Gaussian white noise, $\xi(t)$ and $\zeta(t)$ can be replaced by

$$-\sigma_M\xi(t)\sin\phi + \sigma_A\zeta(t) \rightarrow \sqrt{\sigma_M^2\sin^2\phi - 2\sigma_A\sigma_M R\sin\phi + \sigma_A^2}\,\chi(t)$$

with a Gaussian white noise $\chi(t)$ characterized by

$$\langle\chi(t)\rangle = 0,$$
$$\langle\chi(t)\chi(t')\rangle = \delta(t-t').$$

Then the equation of motion (13) is transformed into

$$\frac{d\phi}{dt} = \omega - b\sin\phi + \sqrt{\sigma_M^2\sin^2\phi - 2\sigma_A\sigma_M R\sin\phi + \sigma_A^2}\chi(t)$$

leading to the Fokker-Planck equation (11) with

$$f(\phi) = \frac{\sigma_M^2\sin\phi\cos\phi - \sigma_A\sigma_M R\cos\phi}{2},$$
$$g(\phi) = \sigma_M^2\sin^2\phi - 2\sigma_A\sigma_M R\sin\phi + \sigma_A^2. \quad (14)$$

Comparing (12) with (14) we can see that the effective Fokker-Planck equation of the active rotator model with nonlinear noises has the same form as that with correlated linear noises providing the multiplicative noise intensity and the correlation parameter as

$$\sigma_M = \sqrt{\Delta_1},$$
$$R = \frac{\Delta_2}{\sqrt{\Delta_1}}.$$

This implies that the nonlinearity of noises may be transformed into the correlation of linear noises.

When $\Delta[\zeta(t)]$ is an even function of $\zeta(t)$, the noise term $-\Delta[\zeta(t)]\sin\phi + \sigma\zeta(t)$ has a symmetry by

$$\phi \to -\phi \text{ and } \zeta(t) \to -\zeta(t) \quad (15)$$

leading to $R = 0$ with $\Delta_2 = 0$. When $\Delta[\zeta(t)]$ is an odd function of $\zeta(t)$, the symmetry (15) is broken leading to nonzero R with nonzero Δ_2. Thus, we can conclude that the correlation comes from the symmetry breaking by the nonlinear noise $\Delta[\zeta(t)]$. Table I shows the values of Δ_1, Δ_2, and R for some nonlinear functions of $\Delta[\zeta]$. In the calculations, we have used the following integration identities [See Appendix]:

$$\int_0^\infty dy\int_0^\infty dz\exp[-(y+z)^2] = \frac{1}{2}, \quad (16)$$
$$\int_0^\infty dy\int_0^\infty dz\frac{\exp[-(y^2+z^2)](1-\exp[-2yz])}{y} = \frac{\sqrt{\pi}\ln 2}{2}. \quad (17)$$

In Fig. 1 we show Δ_1, Δ_2, and R for $\Delta[\zeta] = \mathrm{sgn}[\zeta]|\zeta|^\alpha$ as a function of α. When $\alpha = 0$, Δ_1, Δ_2, and R are 1.39, 1.13, and 0.96, respectively. As α increases up to 1, Δ_1 and Δ_2 decrease and R increases. At $\alpha = 1$, i.e., for the linear case, Δ_1 and Δ_2 have minimum values 1 and R has a maximum value 1. As α increases further, Δ_1 and Δ_2 increase and R decreases. From Fig. 1 we show that the correlation due to the dependence of fluctuation of the threshold on the additive noise is maximized at the linear dependence and the deviation from the linearity reduces the correlation parameter R.

Now, we investigate noise-induced transitions in the system with the nonlinear fluctuation of threshold, $\Delta[\zeta]$. In the steady state, the effective Fokker-Planck equation (11) gives the stationary probability distribution $P(\phi)$ satisfying

$$[\omega - b\sin\phi + f(\phi)]P(\phi) - \frac{1}{2}\frac{d}{d\phi}[g(\phi)P(\phi)] = J, \quad (18)$$

where probability current density J is determined by the boundary condition

$$P(\phi + 2\pi) = P(\phi).$$

Table 1. Values of Δ_1, Δ_2, and R for some nonlinear functions of $\Delta(\zeta)$. Numerical values in parentheses.

$\Delta(\zeta)$	Δ_1	Δ_2	R
$\mathrm{sgn}(\zeta)$	$2\ln 2$ (1.39)	$\frac{2}{\sqrt{\pi}}$ (1.13)	$\sqrt{\frac{2}{\pi \ln 2}}$ (0.96)
ζ	1	1	1
$\mathrm{sgn}(\zeta)\zeta^2$	$\frac{2+\ln 2}{2}$ (1.35)	$\frac{2}{\sqrt{\pi}}$ (1.13)	$\sqrt{\frac{8}{\pi(2+\ln 2)}}$ (0.97)
ζ^3	$\frac{11}{4}$ (2.75)	$\frac{3}{2}$ (1.5)	$\sqrt{\frac{9}{11}}$ (0.91)
$\lvert\zeta\rvert - \frac{1}{\sqrt{\pi}}$	$\frac{\pi - 4 + 2\ln 2}{\pi}$ (0.17)	0	0
$\zeta^2 - \frac{1}{2}$	$\frac{1}{2}$ (0.5)	0	0
$\lvert\zeta\rvert^3 - \frac{1}{\sqrt{\pi}}$	$\frac{33\pi - 64 + 24\ln 2}{12\pi}$ (1.49)	0	0

Here, we consider the fluctuating threshold which depends on the additive noise as its square described by

$$\Delta[\zeta] = \sigma_M \left(\zeta^2 - \frac{1}{2}\right), \tag{19}$$

where 1/2 is subtracted to make $\Delta[\zeta]$ with zero mean. This nonlinear dependence of $\Delta[\zeta]$ on the noise ζ is chosen merely for analytical and numerical convenience. Variation of the nonlinear dependence does not influence the qualitative behavior of the system. From (19), $f(\phi)$ and $g(\phi)$ are given by

$$f(\phi) = \frac{1}{4}\sigma_M^2 \cos\phi \sin\phi,$$
$$g(\phi) = \frac{1}{2}\sigma_M^2 \sin^2\phi + \sigma_A^2.$$

When $\omega = 0$, (11) has the symmetry (15) leading to $J = 0$. Thus, from (18) we obtain

$$\frac{dP(\phi)}{d\phi} = -\frac{\sin\phi(4b + \sigma_M^2 \cos\phi)}{\sigma_M^2 \sin^2\phi + 4\sigma_A^2} P(\phi)$$

showing that when $|4b/\sigma_M^2| > 1$, $P(\phi)$ has a maximum at $\phi = 0$ and a minimum at $\phi = \pi$ producing a single peak in $P(\phi)$. When $|4b/\sigma_M^2| < 1$, $P(\phi)$ has maxima at $\phi = 0$ and π and minima at $\phi_0 \equiv \cos^{-1}(-4b/\sigma_M^2)$ producing two peaks in $P(\phi)$ at $\phi = 0$ and π. Thus, the transition point of the peak-creating transition is given by $\sigma_{Mc} = 2\sqrt{b}$, independent of σ_A. Figure 2 shows $P(\phi)$'s in the one-peak state (solid line with $\sigma_M = b = 1$) and the two-peak state (dashed line with $\sigma_M = 10$ and $b = 1$).

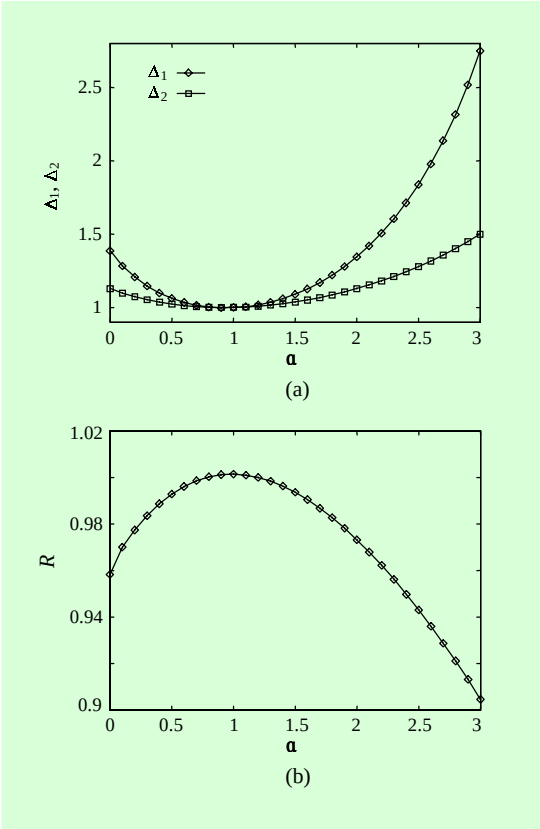

Fig. 1. Plots of Δ_1 (in (a)), Δ_2 (□ in (a)), and R (in (b)) for $\Delta[\zeta] = \mathrm{sgn}(\zeta)|\zeta|^\alpha$ as a function of α. Lines are mere guides to eyes.

IV. COLORED NONLINEAR NOISE

To investigate the colored nonlinear noise effect on the noise-induced transition of the system, we have performed numerical simulations for the system described by (5) with (19) and finite correlation time $\tau \equiv \epsilon^2$. In the simulation, we have used the Euler method with discrete time steps of $\Delta t = 0.0001$ and random initial configurations. At each run, the first 10^7 time steps

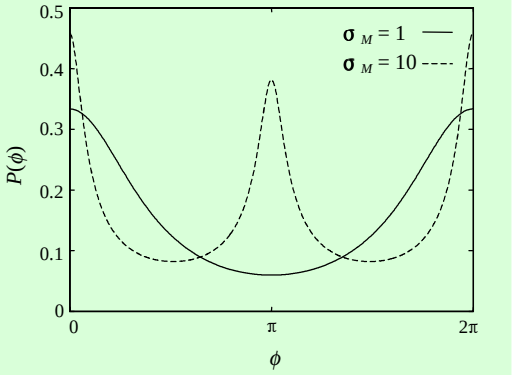

Fig. 2. Plot of $P(\phi)$'s as a function of ϕ: solid line for $\sigma_M = b = 1$ and dashed line for $\sigma_M = 10$ and $b = 1$.

have been discarded to achieve steady state and 10^{10} time steps have been used to compute averages. We have considered the system with $b = 1$ and $\omega = 0$.

Figure 3 shows $P(\phi)$'s obtained by the numerical simulation for various values of σ_M at $b = \epsilon = 1$, $\sigma_A = 2$, and $\omega = 0$. When $\sigma_M = 0$, $P(\phi)$ has a peak at $\phi = 0$. As σ_M increases, peak value $P(0)$ decreases faster than $P(\phi)$ of its neighborhood. Thus, at $\sigma_M = \sigma_{Mc1} \sim 1.0$, $P(\phi)$ has a local minimum at $\phi = 0$ splitting the peak at $\phi = 0$ into two peaks near $\phi = 0$. As σ_M increases up to some value of σ_M, σ_{M1}, the peaks repel each other and the peak values increase. As σ_M increases further, the peaks attract each other and the peak values decrease. At $\sigma_M = \sigma_{Mc2} \sim 3.9$, a peak at $\phi = \pi$ is created showing three peaks in $P(\phi)$. As σ_M increases, the peak value $P(\pi)$ increases and above $\sigma_{Mc3} \sim 6.1$, the peak at $\phi = \pi$

becomes a primary peak among the three peaks.

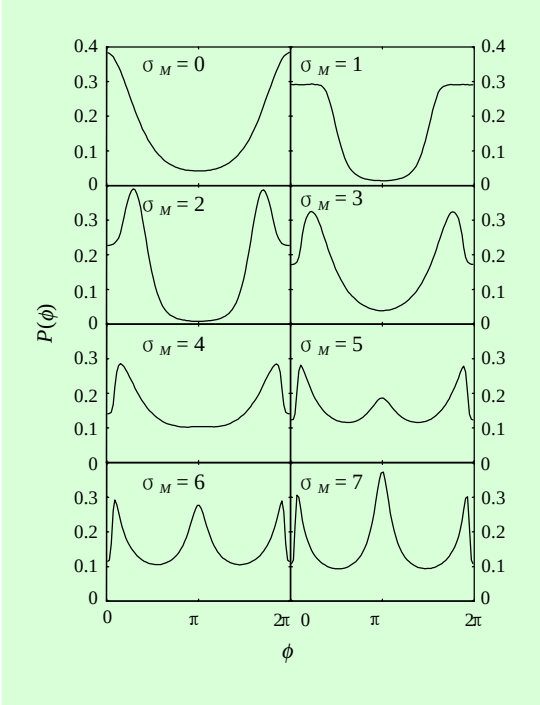

Fig. 3. Plots of probability distribution $P(\phi)$'s at steady state for various values of σ_M obtained by the numerical simulation of (5) with (19) at $b = \epsilon = 1$, $\sigma_A = 2$, and $\omega = 0$.

In Fig. 4, we show $P(\phi)$'s obtained by the numerical simulation for various values of σ_M at $b = \epsilon = 1$, $\sigma_A = 7$, and $\omega = 0$. When $\sigma_M = 0$, $P(\phi)$ has a peak at $\phi = 0$. As σ_M increases, $P(0)$ decreases faster than $P(\phi)$ of its neighborhood. At $\sigma_M = \sigma_{Mc1} \sim 1.8$, $P(\phi)$ has a local minimum at $\phi = 0$ splitting the peak at $\phi = 0$ into two peaks near $\phi = 0$. As σ_M increases, the peaks repel each other and the peak values increase. At $\sigma_M = \sigma_{Mc2} \sim 2.9$, the two peaks meet at $\phi = \pi$ merging into a peak at $\phi = \pi$. As σ_M

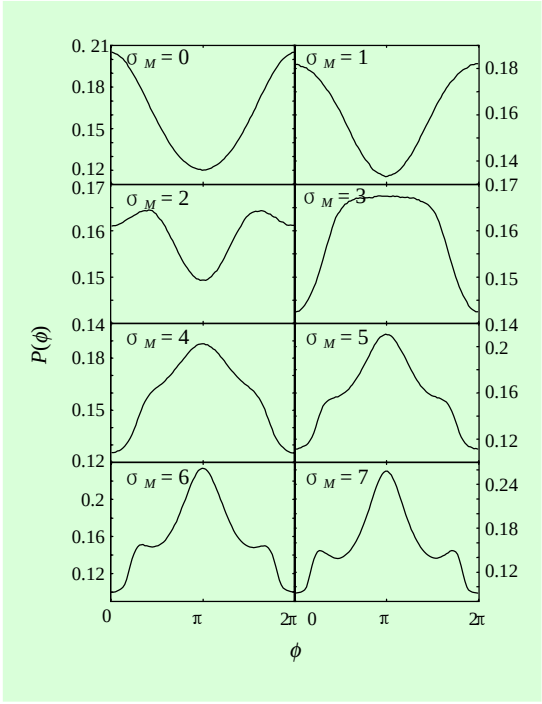

Fig. 4. Plots of probability distribution $P(\phi)$'s at steady state for various values of σ_M obtained by the numerical simulation of (5) with (19) at $b = \epsilon = 1$, $\sigma_A = 7$, and $\omega = 0$.

increases further, $P(\pi)$ increases and two shoulders appear at some values of ϕ, $\phi_\pm$. At $\sigma_M = \sigma_{Mc3} \sim 5.6$, the shoulders change into peaks leading to three peaks with a primary peak at $\phi = \pi$.

Figure 5 shows a phase portrait in σ_A-σ_M plane for the system with (19) at $b = \epsilon = 1$ and $\omega = 0$. In Fig. 5, there are five phases, $P1_0$, $P1_\pi$, $P2_0$, $P3_0$, and $P3_\pi$. $P1_0$ and $P1_\pi$ are one-peak phases with a peak in $P(\phi)$ at $\phi = 0$ and π, respectively, whose typical probability distributions are shown in Fig. 4 with $\sigma_M = 0$ and 3, resepctively. $P2_0$ is a two-peak phase with two peaks in

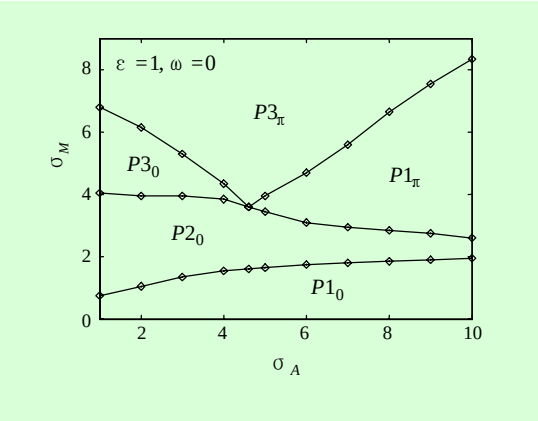

Fig. 5. Plot of phase portrait in σ_A-σ_M plane for the system with (19) at $b = \epsilon = 1$, and $\omega = 0$. $P1_0$ and $P1_\pi$ represent one-peak phases with a peak in $P(\phi)$ at $\phi = 0$ and π, respectively. $P2_0$ means two-peak phase with two peaks in $P(\phi)$ near $\phi = 0$. $P3_0$ and $P3_\pi$ indicate three-peak phases with a primary peak in $P(\phi)$ at $\phi = 0$ and π, respectively. Lines are mere guides to eyes.

$P(\phi)$ near $\phi = 0$, whose typical probability distribution is shown in Fig. 3 with $\sigma_M = 2$. $P3_0$ and $P3_\pi$ are three-peak phases with a primary peak in $P(\phi)$ at $\phi = 0$ and π, respectively, whose typical probability distributions are shown in Fig. 3 with $\sigma_M = 5$ and 7, respectively. For $\sigma_A < \sigma_{Ac} \sim 4.6$, the system shows triple transitions $P1_0 \rightarrow P2_0 \rightarrow P3_0 \rightarrow P3_\pi$ at some values of σ_M, σ_{Mc1}, σ_{Mc2}, and σ_{Mc3}, respectively, as σ_M increases. As σ_A increases, σ_{Mc1} increases and σ_{Mc2} and σ_{Mc3} decrease. For $\sigma_A > \sigma_{Ac}$, there are triple transitions $P1_0 \rightarrow P2_0 \rightarrow P1_\pi \rightarrow P3_\pi$ at some values of σ_M, σ_{Mc1}, σ_{Mc2}, and σ_{Mc3}, respectively, as σ_M increases. As σ_A increases, σ_{Mc1} and σ_{Mc3} increase and σ_{Mc2} decreases. The transitions $P1_0 \rightarrow P2_0$, $P2_0 \rightarrow P3_0$, and $P2_0 \rightarrow P1_\pi$ are peak-splitting, peak-creating, and peak-merging transitions, respectively. The transition $P1_\pi \rightarrow P3_\pi$ is also a peak-creating transition.

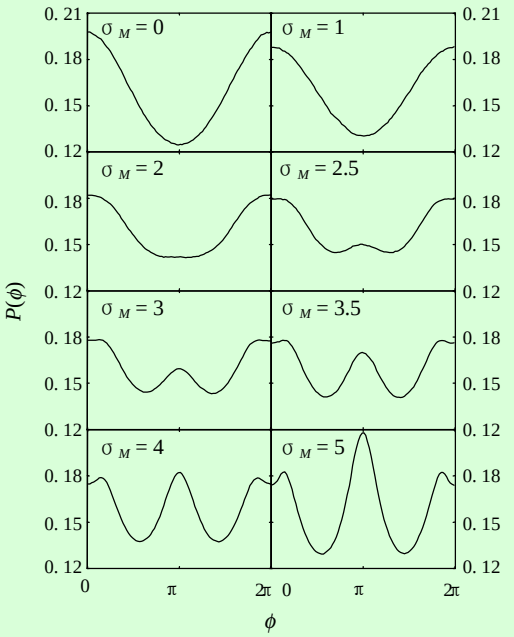

Fig. 6. Plots of probability distribution $P(\phi)$'s at steady state for various values of σ_M obtained by the numerical simulation of (5) with (19) at $b = 1$, $\epsilon = 0.1$, $\sigma_A = 3$, and $\omega = 0$.

Figure 6 shows $P(\phi)$'s obtained by the numerical simulation for various values of σ_M at $b = 1$, $\epsilon = 0.1$, $\sigma_A = 3$, and $\omega = 0$. When $\sigma_M = 0$, $P(\phi)$ has a peak at $\phi = 0$. As σ_M increases, the peak value $P(0)$ decreases. At $\sigma_M = \sigma_{Mc1} \sim 2.1$, a peak at $\phi = \pi$ is created leading to two peaks in $P(\phi)$. As σ_M increases further, the peak

value $P(\pi)$ increases and $P(0)$ decreases faster than $P(\phi)$ of its neighborhood. At $\sigma_M = \sigma_{Mc2} \sim 3.1$, $P(\phi)$ has a local minimum at $\phi = 0$ splitting the peak at $\phi = 0$ into two peaks near $\phi = 0$ and thus the system is in the three-peak phase $P3_0$. For $\sigma_M > \sigma_{Mc3} \sim 3.9$, the peak at $\phi = \pi$ becomes a primary peak among the three peaks leading to the three-peak phase $P3_\pi$.

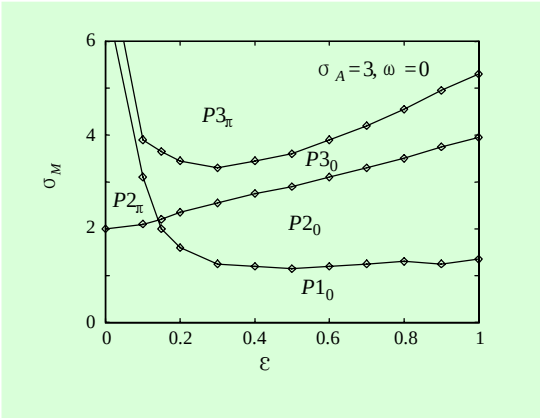

Fig. 7. Plot of phase portrait in ϵ-σ_M plane for the system with (19) at $b = 1$, $\sigma_A = 3$, and $\omega = 0$. $P1_0$ represents a one-peak phase with a peak at $\phi = 0$. $P2_0$ and $P2_\pi$ mean two-peak phases with two peaks near $\phi = 0$ and with two peaks at $\phi = 0$ and π, respectively. $P3_0$ and $P3_\pi$ indicate three-peak phases with a primary peak at $\phi = 0$ and π, respectively. Lines are mere guides to eyes.

Figure 7 shows a phase portrait in ϵ-σ_M plane for the system with (19) at $b = 1$, $\sigma_A = 3$, and $\omega = 0$. In Fig. 7, there are five phases, $P1_0$, $P2_0$, $P2_\pi$, $P3_0$, and $P3_\pi$. $P2_\pi$ represents two-peak phase with two peaks at $\phi = 0$ and π, whose typical probability distribution is shown in Fig. 6 with $\sigma_M =$ 2.5. For $\epsilon < \epsilon_c \sim 0.17$, the system shows triple transitions $P1_0 \to P2_\pi \to P3_0 \to P3_\pi$ at some values of σ_M, σ_{Mc1}, σ_{Mc2}, and σ_{Mc3}, respectively, as σ_M increases. As σ_A increases, σ_{Mc1} increases and σ_{Mc2} and σ_{Mc2} decrease. For $\epsilon > \epsilon_c$, there are triple transitions $P1_0 \to P2_0 \to P3_0 \to P3_\pi$ at some values of σ_M, σ_{Mc1}, σ_{Mc2}, and σ_{Mc3}, respectively, as σ_M increases. As σ_A increases, σ_{Mc1} decreases and σ_{Mc2} and σ_{Mc3} increase. The transitions $P1_0 \to P2_\pi$ and $P2_\pi \to P3_0$ are peak-creating and peak-splitting transitions, respectively.

V. CONCLUSION

In this paper, we have investigated noise-induced transitions in active rotator model with a fluctuating threshold in the presence of an additive noise. We have considered the fluctuating threshold as a nonlinear function of the additive noise. In the white-noise limit, defined by the wide-band limit of the fluctuation $\eta(\phi, \zeta)$, we have obtained the effective Fokker-Planck equation which governs the macroscopic behavior of the system. The effective Fokker-Planck equation has the same form as that of the system with linear fluctuation threshold correlated to the additive noise. This implies that the nonlinearity of the fluctuating threshold may be transformed into the correlation of linear fluctuating threshold. The correlation parameter R reduces as the nonlinearity increases. As an example, we considered square dependent fluctuating threshold with $\Delta[\zeta] = \sigma_M(\zeta^2 - 1/2)$.

In the white-noise limit, the peak-creating transition between one-peak state and two-peak state occurs at $\sigma_{Mc} = 2\sqrt{b}$ independent of the additive noise intensity.

We have also investigated the colored noise effect on the system considering the additive noise as the Ornstein-Uhlenbeck process with a correlation time $\tau = \epsilon^2$. In this case, the system shows six phases, $P1_0$, $P1_\pi$, $P2_0$, $P2_\pi$, $P3_0$ and $P3_\pi$. $P1_0$ and $P1_\pi$ are one-peak phases with a peak at $\phi = 0$ and π, respectively. $P2_0$ and $P2_\pi$ are two-peak phases with two peaks near $\phi = 0$ and with two peaks at $\phi = 0$ and π, resepctively. $P3_0$ and $P3_\pi$ are three-peak phases with a primary peak at $\phi = 0$ and π, respectively. When $\epsilon = 1$, at small intensity of the additive noise, the system shows triple transitions $P1_0 \to P2_0 \to P3_0 \to P3_\pi$ as σ_M increases. While $P1_0 \to P2$ is a peak-splitting transition, $P2_0 \to P3_0$ is a peak-creating transition. At large intensity of the additive noise, the triple transitions $P1_0 \to P2_0 \to P1_\pi \to P3_\pi$ occur as σ_M increases. While $P2_0 \to P1_\pi$ is a peak-merging transition, $P1_\pi \to P3_\pi$ is a peak-creating transition. When ϵ and the additive noise intensity are small, the triple transitions $P1_0 \to P2_\pi \to P3_0 \to P3_\pi$ occur as σ_M increases. While $P1_0 \to P2_\pi$ is a peak-creating transition, $P2_\pi \to P3_0$ is a peak-splitting transition.

In this investigation, we have shown that the nonlinear colored noise produces very peculiar transitions such as the peak-splitting transition, the peak-creating transition, and the peak-merging transition. Since in the case of linear colored noise, only a peak-creating transition occurs, the peak-splitting and the peak-merging transitions are purely nonlinear noise effect. The system with the nonlinear noise $\Delta[\zeta] = \sigma_M(\zeta^2 - 1/2)$ has the symmetry (15), but the linear noise $\Delta[\zeta] = \zeta$ breaks the symmetry (15). This causes the difference between the noise-induced transitions of linear and nonlinear noises.

The active rotator model has been presented as a phenomenological model of oscillatory neurons. The dynamics of the neurons has been described by a phase variable. This description has not considered the origin of the oscillations and has oversimplified the neuronal dynamics. Nevertheless, such an approach is justified at present, because of the lack of experimental guidance on the neuronal dynamics. We introduced the multiplicative noise into the system to simulate the fluctuating threshold of neuronal activity. The multiple peaks in the probability distribution imply the multiple clusters in the weakly coupled active rotator network. Thus, the splitting of peaks in the stationary probability distribution induced by the multiplicative noise may be interpreted by the segmentation of visual scene in visual cortex. Therefore, our results exhibit another route to the segmentation phenomena, which cannot be seen in the deterministic case or in the system with only a simple additive noise. It would be interesting if our results can be tested in physiological systems by observation of the

clustering mechanism of neurons in the visual cortex.

APPENDIX

Firstly, we prove the identities (16) and (17). By the change of variable, $x = y + z$,

$$\Gamma_1 \equiv \int_0^\infty dy \int_0^\infty dz \exp\left[-(y+z)^2\right]$$

reduces to

$$\begin{aligned}\Gamma_1 &= \int_0^\infty dx \int_0^x dy \exp\left[-x^2\right] \\ &= \int_0^\infty dx \exp\left[-x^2\right] x \\ &= \frac{1}{2}.\end{aligned}$$

By the expansion of $\exp[-2yz]$ as a polynomial of $2yz$,

$$\begin{aligned}\Gamma_2 \equiv \int_0^\infty dy \int_0^\infty dz \frac{1}{y} \exp\left[-(y^2+z^2)\right] \\ \times(1-\exp[-2yz])\end{aligned}$$

reduces to

$$\begin{aligned}\Gamma_2 = \sum_{n=1}^\infty \frac{(-1)^{n+1}2^n}{n!} \int_0^\infty dy \exp\left[-y^2\right] y^{n-1} \\ \times \int_0^\infty dz \exp\left[-z^2\right] z^n.\end{aligned}$$

Using the integration identities

$$\int_0^\infty x^{2n+1} \exp\left[-x^2\right] dx = \frac{n!}{2},$$
$$\int_0^\infty x^{2n} \exp\left[-x^2\right] dx = \frac{(2n-1)!!}{2^{n+1}}\sqrt{\pi},$$

we obtain

$$\begin{aligned}\Gamma_2 &= \sqrt{\pi}\sum_{n=0}^\infty \left[\frac{2^{n-1}n!}{(2n+1)(2n)!!} - \frac{2^n n!}{2(2n+2)!!}\right] \\ &= \frac{\sqrt{\pi}}{2}\sum_{n=0}^\infty \left(\frac{1}{2n+1} - \frac{1}{2n+2}\right) \\ &= \frac{\sqrt{\pi}}{2}\sum_{n=0}^\infty \frac{(-1)^{n+1}}{n} \\ &= \frac{\sqrt{\pi}}{2}\ln 2.\end{aligned}$$

Using the identities, $\Gamma_1 = 1/2$ and $\Gamma_2 = \sqrt{\pi}\ln 2/2$, we calculate Δ_1 and Δ_2 in Table I. When $\Delta[\zeta] = \mathrm{sgn}[\zeta]$, Δ_1 is given by

$$\begin{aligned}\Delta_1 = \frac{8}{\sqrt{\pi}} \int_0^\infty d\zeta \exp\left[-\zeta^2\right] \int_0^\zeta d\zeta' \exp\left[\zeta'^2\right] \\ \times \int_{\zeta'}^\infty d\zeta'' \exp\left[-\zeta''^2\right].\end{aligned}$$

By the change of variables, $\zeta' + \zeta'' = x$ and $\zeta' - \zeta'' = -y$ we obtain

$$\begin{aligned}\Delta_1 &= \frac{4}{\sqrt{\pi}} \int_0^\infty d\zeta \exp\left[-\zeta^2\right] \int_0^\infty dy \\ &\quad \times \int_y^{2z+y} dx \exp[-xy] \\ &= \frac{4}{\sqrt{\pi}} \int_0^\infty d\zeta \exp\left[-\zeta^2\right] \\ &\quad \times \int_0^\infty dy \frac{\exp[-y^2]}{y}(1-\exp[-2\zeta y]) \\ &= \frac{4}{\sqrt{\pi}}\Gamma_2 \\ &= 2\ln 2.\end{aligned}$$

By direct integration we obtain $\Delta_2 = 2/\sqrt{\pi}$.

When $\Delta[\zeta] = \zeta$, to show $\Delta_1 = \Delta_2 = 1$ is easy.

When $\Delta[\zeta] = \mathrm{sgn}[\zeta]\zeta^2$, by integrations by parts

$$\begin{aligned}\Delta_1 = \frac{8}{\sqrt{\pi}} \int_0^\infty d\zeta \exp\left[-\zeta^2\right] \zeta^2 \int_0^\zeta d\zeta' \exp\left[\zeta'^2\right] \\ \times \int_{\zeta'}^\infty d\zeta'' \exp\left[-\zeta''^2\right] \zeta''^2\end{aligned}$$

reduces to

$$\Delta_1 = 1 + \frac{\Gamma_2}{\sqrt{\pi}}$$

leading to $\Delta_1 = (2+\ln 2)/2$. By direct integration $\Delta_2 = 2/\sqrt{\pi}$.

When $\Delta[\zeta] = \zeta^3$, using

$$\int_{\zeta'}^{\infty} d\zeta'' \exp\left[-\zeta''^2\right] \zeta''^3 = \frac{1}{2}(\zeta'^2 + 1)\exp\left[\zeta'^2\right],$$

we obtain $\Delta_1 = 11/4$ and by integrations by parts $\Delta_2 = 3/2$.

Following the same procedure, we obtain

$$\Delta_1 = \begin{cases} 1 - 2(2-\ln 2)/\pi \\ \qquad \text{for } \Delta[\zeta] = |\zeta| - 1/\sqrt{\pi} \\ 1/2 \\ \qquad \text{for } \Delta[\zeta] = \zeta^2 - 1/2 \\ (33\pi - 64 + 24\ln 2)/12\pi \\ \qquad \text{for } \Delta[\zeta] = \zeta^3 - 1/\sqrt{\pi}. \end{cases}$$

ACKNOWLEDGMENT

This work was supported by the Ministry of Information and Communications, Korea. We are grateful to Dr. E. H. Lee for his support on this research.

REFERENCES

[1] C. von der Malsburg and W. Schneider, "A Neural Cocktail-Party Processor," *Biol. Cybern.*, Vol. 54, 1986, pp. 29-40.

[2] R. Eckhorn, R. Bauer, W. Jordan, M. Brosch, W. Kruse, M. Munk, and R.J. Reitboeck, "Coherent Oscillations: A Mechanism of Feature Linking in the Visual Cortex," *Biol. Cybern.*, Vol. 60, 1988, pp. 121-130.

[3] C.M. Gray, P. Konig, A.K. Engel, and W. Singer, "Oscillatory Responses in Cat Visual Cortex Exhibit Inter-Columnar Synchronization Which Reflects Global Stimuli Properties," *Nature*, Vol. 338, 1989, pp. 334-337.

[4] H. Sompolinsky, D. Golomb, and D. Kleinfeld, "Cooperative Dynamics in Visual Processing," *Phys. Rev. A*, Vol. 43, 1991, pp. 6990-7011.

[5] S. Kim and M.Y. Choi, "Arrays of Resistively Shunted Josephson-Junctions in Magnetic Fields," *Phys. Rev. B*, Vol. 48, 1993, pp. 322-332.

[6] Y. Kuramoto, *Chemical Oscillations, Waves, and Turbulence*, Springer, New York, 1984, pp. 1-326.

[7] D. Fisher, "Sliding Charge-Density Waves as a Dynamic Critical Phenomena," *Phys. Rev. B*, Vol. 31, 1985, pp. 1396-1427.

[8] S.H. Strogatz, C.M. Marcus, R.M. Westervelt, and R.E. Mirollo, "Collective Dynamics of Coupled Oscillators with Random Pinning," *Physica D*, Vol. 36, 1989, pp. 23-50.

[9] S. Shinomoto and Y. Kuramoto, "Phase Transitions in Active Rotator Systems," *Prog. Theor. Phys.*, Vol. 75, 1986, pp. 1105-1110.

[10] R.L. Stratonovich, *Topics in the Theory of Random Noise*. Gordon and Breach Science Publisher, New York, 1967.

[11] Y. Yamaguchi and H. Shimizu, "Pattern Recognition with Figure-Ground Separation by Generation of Coherent Oscillations," *Neural Networks*, Vol. 7, 1994, pp. 49-63.

[12] Y. Hirakura, Y. Yamaguchi, H. Shimizu, and S. Nagai, "Dynamic Linking Among Neural Oscillators Leads to Flexible Pattern Recognition with Figure-Ground Separation," *Neural Networks*, Vol. 9, 1996, pp. 198-209.

[13] W. Horsthemke and R. Lefever, *Noise-Induced Transitions*. Springer-Verlag, New York, 1984, pp. 1-318.

[14] C. Van den Broeck, J.M.R. Parrondo, J. Armero, and A. Hernández-Machado, "Mean Field Model for Spatially Extended Systems in the Presence of Multiplicative Noise," *Phys. Rev. E*, Vol. 49, 1994, pp. 2639-2643.

[15] C. Van den Broeck. J.M.R. Parrondo, and R. Toral, "Noise-Induced Nonequilibrium Phase Transition," *Phys. Rev. Lett.*, Vol. 73, 1994, pp. 3395-3398.

[16] I.I. Fedchenia and N.A. Usova, "Noise Competition in a Nonlinear System: I. Two Indenpendent Noises," *Z. Phys. B – Condense Matter*, Vol. 50, 1983, pp. 263-267.

[17] I.I. Fedchenia and N.A. Usova, "Noise Competition in a Nonlinear System: I. Two Indenpendent Noises," *Z. Phys. B – Condense Matter*, Vol. 52, 1983, pp. 69-73.

[18] S. Kim, S.H. Park, and C.S. Ryu, "Noise-Induced Transitions in Coupled Oscillator Systems with a Pinning Force," *Phys. Rev. E*, Vol. 54, 1996, pp. 6042-6052.

[19] S. Kim, S.H. Park, and C.S. Ryu, "Nonequilibrium Phenomena in Globally Coupled Active Rotators with Multiplicative and Additive Noises," *ETRI J.*, Vol. 18, 1996, pp. 147-160.

[20] S. Kim, S.H. Park, and C.S. Ryu, "Noise-Enhanced Multistability in Coupled Oscillator Systems," *Phys. Rev. Lett.*, Vol. 78, 1997, pp. 1616-1619.

[21] S. Kim, S.H. Park, and C.S. Ryu, "Comment on Noise-Induced Nonequilibrium Phase Transition," *Phys. Rev. Lett.*, Vol. 78, 1997, p. 1827.

[22] S. Kim, S.H. Park, C.R. Doering, and C.S. Ryu, "Reentrant Transitions in Globally Coupled Active Rotators with Multiplicative and Additive Noises," *Phys. Lett. A*, Vol. 224, 1997, pp. 147-153.

[23] S. Kim, S.H. Park, and C.S. Ryu, "The Fokker-Planck Equation for Arbitrary Nonlinear Noises," *Phys. Lett. A*, Vol. 229, 1997, pp. 190-194.

[24] G. Blankenship and G.C. Papanicolaou, "Stability and Control of Stochastic Systems with Wide-Band Noise Disturbances. I," *SIAM J. Appl. Math.*, Vol. 34, 1978, pp. 437-476.

[25] H. Risken, *The Fokker-Planck Equation*, Springer-Verlag, New York, 1988, pp. 1-426.

Seunghwan Kim received his B.S., M.S., and Ph.D. degrees in Physics (condensed matter theory) from Seoul National University in 1988, 1990, and 1995, respectively. He had worked extensively in the field of phase trasitions and dynamics of Josephosn-junction arrays. In 1995, he joined the Research Department at ETRI as a postdoc and after a year he became a member of the staff. Currently, he has worked on the new information processing method based on the collective dynamics of biological neurons in the nervous system and brain. Up to now, he published three dozens of papers in the journals of Physical Review Letters, Physical Review B and E, Europhysics Letters, Journal of Physics A, etc.

Seon Hee Park receive the B.S. degree from Seoul National University, College of Education, with mathematics major in 1981. She received he M.A. and Ph.D. degree from the University of Texas at Austin in USA in 1986 and 1989, respectively on quantum field theories. In the following four years she worked as a postdoc at three places: Center for Relativity at the University of Texas at Austin USA, International Center for Theoretical Physics in Italy, and Center for Theoretical Physics at Seoul National University. In 1994 she joined the Research Department at ETRI. She has worked extensively in the field of non-perturbative approach to various quantum field theories, and published dozens of papers in the journals of Physical Review Letters, Physics Report, Nuclear Physics, etc. Currently she has a research interest on the new informatics based on the collective dynamics occurring in the biological nerve and brain systems.

Chang Su Ryu received his B.S., M.S., and Ph.D. degrees in physics (solid state theory) from Seoul Nationl University in 1985, 1988, and 1993, respectively. His main interest had lain in electronic properties of partially disordered systems. He spent two years at Korea University to study the kinetic roughening in epitaxial growth as a postdoc. Since his joining ETRI in 1995, he has worked on modeling of memory at mole-cular level and nonlinear dynamical analysis of biological signal to understand information processing in human brain.